Composition, seasonal change and bathymetry of Ligeia Mare, Titan, derived from its microwave thermal emission

Alice Le Gall, M.J. Malaska, R.D. Lorenz, M.A. Janssen, T. Tokano, A.G. Hayes, M. Mastrogiuseppe, J.I. Lunine, Gaëlle Veyssière, P. Encrenaz, et al.

AGU PUBLICATIONS

JGR

Journal of Geophysical Research: Planets

RESEARCH ARTICLE
10.1002/2015JE004920

Key Points:
- Radiometry observations of Ligeia Mare support a liquid composition dominated by methane
- The seafloor of Ligeia Mare probably consists of a sludge of compacted organic-rich material
- No significant net cooling from 2007 to 2013 but possible lag in the summer warming in the north

Correspondence to:
A. Le Gall,
Alice.Legall@latmos.ipsl.fr

Citation:
Le Gall, A., et al. (2016), Composition, seasonal change, and bathymetry of Ligeia Mare, Titan, derived from its microwave thermal emission, *J. Geophys. Res. Planets*, *121*, doi:10.1002/2015JE004920.

Received 7 AUG 2015
Accepted 17 JAN 2016
Accepted article online 20 JAN 2016

Composition, seasonal change, and bathymetry of Ligeia Mare, Titan, derived from its microwave thermal emission

A. Le Gall[1], M. J. Malaska[2], R. D. Lorenz[3], M. A. Janssen[2], T. Tokano[4], A. G. Hayes[5], M. Mastrogiuseppe[5], J. I. Lunine[5], G. Veyssière[6], P. Encrenaz[7], and O. Karatekin[8]

[1]LATMOS/IPSL, UVSQ Université Paris-Saclay, UPMC Univ. Paris 06, CNRS, Guyancourt, France, [2]Jet Propulsion Laboratory, California Institute of Technology, Pasadena, California, USA, [3]The Johns Hopkins University Applied Physics Laboratory, Laurel, Maryland, USA, [4]Institut für Geophysik und Meteorologie, Universität zu Köln, Cologne, Germany, [5]Carl Sagan Institute, Department of Astronomy and CCAPS, Cornell University, Ithaca, New York, USA, [6]Centre d'Etudes de la Neige, Grenoble, France, [7]Laboratoire d'Etudes du Rayonnement et de la Matière en Astrophysique et Atmosphères, Observatoire de Paris-Meudon, Paris, France, [8]Royal Observatory of Belgium, Uccle, Belgium

Abstract For the last decade, the passive radiometer incorporated in the Cassini RADAR has recorded the 2.2 cm wavelength thermal emission from Titan's seas. In this paper, we analyze the radiometry observations collected from February 2007 to January 2015 over one of these seas, Ligeia Mare, with the goal of providing constraints on its composition, bathymetry, and dynamics. In light of the depth profile obtained by Mastrogiuseppe et al. (2014) and of a two-layer model, we find that the dielectric constant of the sea liquid is <1.8, and its loss tangent is $< 3.6^{+4.3}_{-2.1}\times10^{-5}$. Both results point to a composition dominated by liquid methane rather than ethane. A high methane concentration suggests that Ligeia Mare is primarily fed by methane-rich precipitation and/or ethane has been removed from it (e.g., by crustal interaction). Our result on the dielectric constant of the seafloor is less constraining $\left(< 2.9^{+0.9}_{-0.9}\right)$, but we favor a scenario where the floor of Ligeia Mare is covered by a sludge of compacted and possibly nitrile-rich organic material formed by the deposition of photochemical haze or by rain washing of the nearby shores. We use these results to produce a low-resolution bathymetry map of the sea. We also estimate the temperature variation of the bulk sea between February 2007 and July 2013 to be <2 K, which provides a constraint on its net evaporative cooling currently being explored in ocean circulation models. Lastly, we suggest a lag in the summer warming of the northern polar terrains.

1. Introduction

Saturn's moon Titan is the only planetary body besides Earth whose surface presently exhibits significant accumulations of stable liquids in the forms of lakes and seas. The presence of hydrocarbon lakes and seas on Titan was anticipated long before the launch of the Cassini mission [e.g., *Lunine et al.*, 1983], but the synthetic aperture radar (SAR) on board Cassini observed them unequivocally for the first time in 2006 [*Stofan et al.*, 2007]. Cassini discovered hundreds of radar-dark lake-like features of various sizes in the north polar terrains of Titan but only one major lake, Ontario Lacus with a surface area of 15,600 km^2, in the south [*Turtle et al.*, 2009; *Barnes et al.*, 2009; *Hayes et al.*, 2008, 2010]. Among these bodies of standing liquid, three are large enough to deserve to be called "seas": Kraken Mare (~490,000 km^2) [*Turtle et al.*, 2009], Ligeia Mare (~126,000 km^2) [*Hayes et al.*, 2008], and Punga Mare (49,000 km^2) [*Hayes et al.*, 2008]. This paper is dedicated to Ligeia Mare.

Though the Titan's polar seas and lakes are thought to be primarily composed of liquid methane, and ethane (probably mixed with dissolved atmospheric nitrogen), the relative abundance of these hydrocarbons in the lakes and seas has, until recently, remained elusive. While the visible and infrared mapping spectrometer (VIMS) on board Cassini detected the spectral signature of ethane in Ontario Lacus [*Brown et al.*, 2008], the data were not sufficient to permit determination of abundance. Meanwhile, direct detection of methane liquid on Titan's surface is not possible with Cassini due to methane's strong atmospheric absorption. Knowing the composition of the seas and lakes of Titan, as well as the volume of liquid they contain, is essential to a firm understanding of their formation and dynamics and hence of the carbon cycle on Titan.

Toward that effort, passive microwave radiometry can be a powerful complement to active radar backscatter measurements or remote sensing at shorter wavelengths, providing independent constraints on both the

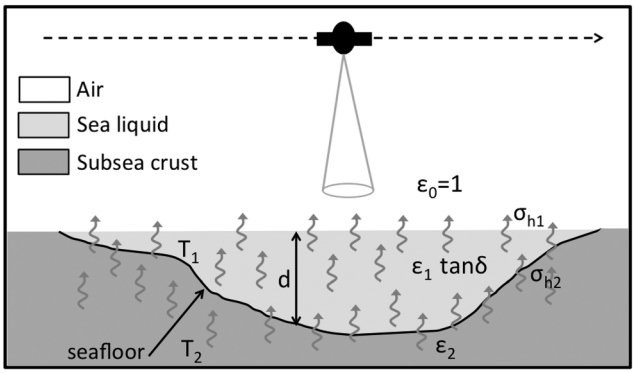

Figure 1. Two-layer model for modeling the microwave thermal emission from Titan's seas and lakes. ε_1 and ε_2 are the dielectric constants of the liquid layer and the bottom of the sea, respectively. tan δ is the loss tangent of the liquid layer. σ_{h1} and σ_{h2} are the RMS height of the surface and bottom of the sea, respectively. The instrument is here shown in a nadir-looking (or altimetry) geometry; the incidence and transmitted angles (θ and θ' in section 2) are therefore both equal to 0°.

composition and bathymetry of the lakes [*Lorenz et al*., 2003] and possible evidence for evaporative cooling. For the last 10 years, the radiometer incorporated in the Cassini RADAR instrument [*Elachi et al*., 2004] has observed the thermal microwave emission from Titan's surface at a wavelength of 2.2 cm. The radiometry global mosaic first published in *Janssen et al*. [2009] has recently been updated to include all data accumulated through February 2014, and its calibration refined to an unprecedented accuracy of ~1% [*Janssen et al*., 2016]. This paper aims to extract all scientific information on Ligeia Mare using this new data set, the analysis of which has already proved to be valuable in understanding Titan's geological features. In particular, radiometry observations provide a further argument for the organic composition of Titan's dune fields and revealed the likely origin of their regional variations [*Le Gall et al*., 2011, 2012].

Ligeia Mare is the first sea/lake of Titan for which a depth profile—or bathymetry profile—was generated. *Mastrogiuseppe et al*. [2014] constructed this profile from altimeter data collected by the Cassini RADAR during the 91st flyby of the moon (hereafter referred to as T91). During this pass, the instrument detected echoes reflected both from the surface and from the bottom of the sea and the difference in time of arrival of these echoes was used to retrieve the thickness of the liquid layer along the T91 altimetry track. They determined a maximum depth of ~160 m along the observed transect. *Mastrogiuseppe et al*. [2014] and Mastrogiuseppe et al. (RADAR sounding using Cassini altimeter: Waveform modeling and Monte Carlo approach for data inversion of observation of Titan liquid bodies, submitted to *IEEE Geoscience and Remote Sensing*, 2016) also investigated the difference of amplitude of the surface and bottom echoes in order to evaluate losses by absorption in the liquid layer. They found a (very low) value of $(4.8 \pm 1.0) \times 10^{-5}$ for the loss tangent, which suggests a methane-dominated composition, based on comparison with laboratory data acquired by *Mitchell et al*. [2015]. It is the extreme transparency of the sea liquid to microwaves that allows the radiometer (and the radar) to sample depths as great as several thousand times its operating wavelength.

In this paper, particular attention is paid to the analysis of the passive radiometry data that were acquired during the T91 altimetry pass, concurrently with the active data. Our objectives are to provide an independent estimate of the liquid loss tangent and to determine the respective dielectric constants of the liquid and seafloor. All other available high spatial resolution observations are considered to support this analysis (see section 3), which is based on a two-layer model described in section 2 and uses the bathymetry profile obtained by *Mastrogiuseppe et al*. [2014]. We also examined the data to search for potential seasonal changes. Our results are discussed in section 4 and used to convert the radiometry mosaic of Ligeia Mare into a qualitative low-resolution bathymetry map.

2. A Two-Layer Model for Titan's Seas

A schematic two-layer model for Titan's seas and lakes (for the sake of simplicity, the descriptor "sea" will be used for both lake and sea in the remainder of the paper) is shown in Figure 1. The brightness temperatures measured above the sea should consist of two contributions:

$$T_b(\theta;p) = T_{b1}(\theta;p) + T_{b2}(\theta;p) \quad (1)$$

where T_{b1} represents the thermal emission from the sea liquid, T_{b2} is the thermal emission from the sea bottom attenuated in the liquid layer, θ is the emission angle, and p is the polarization.

More specifically, assuming smooth boundaries between the air and the sea liquid and the sea liquid and the bottom and considering only losses by absorption in the sea liquid, *Ulaby et al.* [1982a] show that T_b can be expressed as

$$T_b(\theta;p) = \frac{1-\Gamma_1}{1-\Gamma_1\Gamma_2 L_1^2}[(1+\Gamma_2 L_1)(1-L_1)T_1 + (1-\Gamma_2)L_1 T_2] \quad (2)$$

Γ_1 and Γ_2 are the Fresnel reflection coefficients (or specular reflectivities) at the boundaries air/liquid and liquid/bottom, respectively. They depend on the permittivity of the media they separate, on the polarization and on the emission angle at the boundaries, respectively, θ and θ' where θ' is the angle of transmission in the liquid layer given by

$$\theta' = \sin^{-1}(\sin\theta/\sqrt{\varepsilon_1}) \quad (3)$$

where ε_1 is the relative dielectric constant (real part of the complex permittivity normalized by the permittivity of the void ε_0) of the liquid layer.L_1 represents the (exponential) attenuation of the electromagnetic waves by absorption in the liquid layer. It is defined as

$$L_1 = e^{-\frac{d}{\delta_e \cos\theta'}} \quad (4)$$

where d is the thickness of the liquid layer (i.e., the depth of the seafloor) and δ_e is the electrical skin depth at the wavelength of operation λ (2.2 cm for the Cassini RADAR):

$$\delta_e = \frac{\lambda}{4\pi}\left(\frac{\varepsilon_1}{2}\left(\sqrt{1+\tan^2\delta}-1\right)\right)^{-1/2} \quad (5)$$

$\tan\delta$ is the loss tangent of the liquid material (ratio between the imaginary and the real parts of the liquid permittivity). The smaller the loss tangent, the larger the electrical skin depth and thus the larger the depth to which the instrument senses the subsurface. On the contrary, if losses are large, the emission from the seafloor will be masked even by a thin layer of liquid. The model does not account for losses by scattering that would occur if centimeter-sized particles were suspended within the liquid layer. Such losses have been found to be negligible in Ligeia Mare [*Mastrogiuseppe et al.*, 2014], and the liquid layer can reasonably be considered as uniform. The seafloor is here assumed homogeneous and infinite in depth.Lastly, T_1 and T_2 are the physical temperatures of the sea liquid and sea bottom, respectively. If the sea is isothermal ($T_1 = T_2$), its net emissivity can be expressed as follows:

$$e(\theta;p) = \frac{1-\Gamma_1}{1-\Gamma_1\Gamma_2 L_1^2}[(1+\Gamma_2 L_1)(1-L_1) + (1-\Gamma_2)L_1] \quad (6)$$

The two-layer model incorporates all multiple reflections at the two boundaries.

The effect of surface scattering by small-scale roughness (i.e., roughness related to surface irregularities, small compared to the wavelength) can be further included by modifying the Fresnel reflection coefficients, Γ_1 and Γ_2, by a single-parameter roughness factor (respectively termed f_1 or f_2) such as proposed by *Choudhury et al.* [1979]:

$$\Gamma_{ri} = f_i\Gamma_i \text{ with } f_i = e^{-4\left(\frac{2\pi\sqrt{\varepsilon_{i-1}}}{\lambda}\right)^2\sigma_{hi}^2\cos^2\theta_i}, \quad i = 1 \text{ or } 2, \quad \theta_1 = \theta \text{ and } \theta_2 = \theta' \quad (7)$$

where σ_{hi} is the RMS (root-mean-square) surface height of the interface i. This simple law expresses how an increasing small-scale surface roughness results in a corresponding increase in the surface emissivity. However, in practice, it was shown that equation (7) tends to exaggerate the effect of roughness [*Ulaby et al.*, 1982b]. More specifically, in the case reported by *Choudhury et al.* [1979], the RMS surface height derived from surface-scattering models had to be divided by a factor of 3 in order to fit measured data. Moreover, the law described by equation (7) was established for moist solid terrains and likely does not apply to Titan's sea surfaces. For all these reasons, it must be used only as a guideline.

Though the composition of the seas may vary across Titan, the relative dielectric constant ε_1 of the liquid they contain most probably lies in the range 1.6–2.0, based on laboratory measurements of liquid hydrocarbons [*Lorenz et al.*, 2003; *Paillou et al.*, 2008; *Mitchell et al.*, 2015]. From the laboratory work, the loss tangent of the liquid layer $\tan\delta$ is expected to be small. It was estimated to be $9.2^{+2.5}_{-2.0}\times10^{-4}$ in the nearshore region of Ontario Lacus using an assumed bathymetry profile and SAR backscatter variations [*Hayes et al.*, 2010] and $(4.8\pm1.0)\times10^{-5}$ for the bulk of Ligeia Mare using active altimetry data

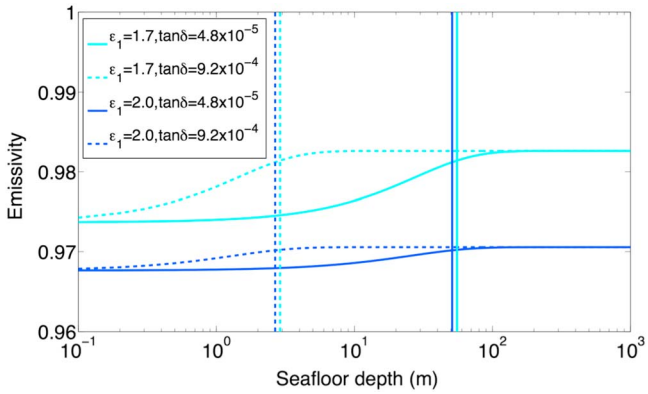

Figure 2. Emissivity at normal incidence over a Titan sea as a function of the depth of the seafloor as predicted by the two-layer model described in section 2 for different liquid compositions (i.e., different liquid dielectric constants ε_1 and loss tangents tan δ). The surfaces of the sea and of the seafloor are assumed to be smooth. The dielectric constant of the seafloor is set to 2.5. The vertical solid lines indicate the electrical skin depth corresponding to each tested composition.

(Mastrogiuseppe et al., submitted manuscript, 2016, updated from the value of $(3.0 \pm 1.0) \times 10^{-5}$ first published in *Mastrogiuseppe et al.* [2014]). For this latter result, the corresponding electrical skin depth is ~60 m (see equation (5)). This is almost 3000 times the operating wavelength! Active altimetry measurements by Cassini over Ligeia Mare also show very strong specular radar reflections at the surface of the sea, constraining surface height variations to 1 mm RMS [*Zebker et al.*, 2014]. The same type of data acquired over Ontario Lacus provided an upper bound for the RMS surface height variation to be 3 mm [*Wye et al.*, 2009]. As previously mentioned, these radar-derived RMS surface heights must be reduced by some factor before being introduced in equation (7). Lastly, in the absence of indication to the contrary, the emission from the seafloor is assumed to be similar to the emission from the nearby shore where the dielectric constant was found to be from 2.2 to 2.4 around Ligeia Mare [*Zebker et al.*, 2014].

Because a larger dielectric constant implies a smaller emissivity, the bottom of the seas is a priori less emissive than the liquid layer, and the net emissivity measured over Titan's marine features should increase as the depth of the sea increases, i.e., as the contribution from the bottom diminishes. Figure 2 illustrates the expected variations of the emissivity with the seafloor depth for parameter values in the ranges previously described and assuming an isothermal sea. The assumed dielectric contrast between the liquid and the bottom being small, the emissivity is expected to vary across Titan's sea by at most 1%. The smaller the loss tangent, the larger the mean depth of the 2.2 cm emission and therefore the longer (in depth) it takes for the emissivity to reach saturation. Saturation is eventually reached once the sea bottom is deep enough so that its microwave thermal emission does not arise at the surface anymore. Lastly, though not shown here, it can be also noted that a sea surface displaying subwavelength-scale irregularities is slightly more emissive than a perfectly smooth one.

3. Cassini Microwave Radiometry Observations

3.1. Cassini Radiometry Observations of Titan's Surface

The passive radiometer incorporated in the RADAR on board the Cassini records the thermal microwave emission from Titan through the measurement of its surface brightness temperature T_b at the wavelength of 2.2 cm. There are two types of radiometry data products (available on Planetary Data System (PDS) as the Short Burst Data Record (SBDR) products):

1. The global radiometry map mosaicked from all individual radiometry observations taken at a variety of resolutions, emission angles, and epochs since the first Titan pass in October 2004. These observations were combined together after adjustment to a common incidence angle (normal incidence) and epoch (Titan's vernal equinox, i.e., 11 August 2009). The resulting map is now complete; it covers all Titan with resolution ranging from 5 to 500 km.
2. Individual high spatial resolution radiometry data sets acquired either in the SAR or altimetry (nadir-looking) mode of the RADAR instrument which are used at altitudes under ~4000 km. These observations are incorporated into the global radiometry map previously mentioned. Their resolution generally ranges from 5 to 50 km.

The approach used for the calibration and mapping of the radiometry observations is described in *Janssen et al.* [2009]. It has been recently refined and updated, now including all the observations accumulated through February 2014 [*Janssen et al.*, 2016]. The redundancy in the mapping was used to estimate systematic errors

Table 1. Cassini High Spatial Radiometry Observations of Ligeia Mare From February 2007 to January 2015

Pass	Date	Solar Longitude L_s (deg)	Areal Coverage of the Sea[a] (%)	Emission Angle Range (deg)	Polarization Angle Range[b] (deg)	Range of the Size of the Footprint[c] (km × km)	Averaged Emissivity at Normal Incidence[d]
T25	22 Feb 2007	331	92.8	15.0–20.0	196–237	(26–34) × (26–136)	0.985 ± 0.004
T28	10 Apr 2007	333	36.3	13.5–19.5	167–180	(15–19) × (15–79)	0.992 ± 0.004
T29	26 Apr 2007	334	56.3	16.5–23.5	170–179	(12–15) × (12–75)	0.993 ± 0.005
T64[e]	24 Dec 2009	4	29.7	31.5–38.5	~180	(7–9) × (7–46)	0.986 ± 0.007
T86	26 Sep 2012	37	30.7	35.5–42.0	24–42	(9–10) × (9–52)	0.980 ± 0.005
T91	23 May 2013	42	<1	0	-	(10–12) × (10–12)	0.981 ± 0.004
T92	10 Jul 2013	43.5	57.7	5.0–15.5	0–17	(12–17) × (12–77)	0.989 ± 0.007
T104	21 Aug 2014	58	78.9	4.0–12.0	357–3	(23–27) × (23–113)	0.972 ± 0.003[f]
T108	11 Jan 2015	61	39.0	2.3–11.5	194–242	(9–11) × (9–48)	0.970 ± 0.004[f]

[a]The area covered by the small islands embedded within the seas/lakes was removed for the derivation of the sea areal coverage.
[b]Angle is 0° (modulo 180°) in perpendicular polarization and 90° (modulo 180°) in parallel polarization.
[c]Minimum and maximum sizes of the radiometry footprints along and across the swath.
[d]The emissivity of Ligeia Mare is obtained using equation (8) and averaging measurements that were performed only in radiometry footprints lying entirely with the sea. These values are accurate to 1% [*Janssen et al.*, 2016]. The statistical uncertainties based on the dispersion of measurements for each pass are indicated.
[e]Data were partially lost during flyby T64 due to Deep Space Network failure.
[f]This emissivity value is subject to caution because there is no reliable model available for the effective temperature after December 2013 (i.e., equation (9) is most probably not valid anymore).

in the brightness mosaic to be less than 1%. The relative precision within individual data sets, as long as the geometry of observation does not change too much, is at least twice smaller, as supported by the standard deviations of the emissivity values reported in Table 1. Lastly, the net uncertainty associated with the absolute calibration process is estimated to be about 1%.

The measured 2.2 cm surface brightness temperatures provide insights into the thermal, physical, and chemical properties of the surface to depths of centimeters to meters. In the microwave domain, because the Rayleigh-Jeans approximation applies, the brightness temperatures can be converted into emissivity, a measure of the surface's ability to radiate the absorbed energy, as follows:

$$e(\theta;p) = \frac{T_b(\theta;p)}{T_{\text{eff}}} \tag{8}$$

where θ is the angle of observation/emission, p denotes the polarization, and T_{eff} is the effective temperature sensed by the radiometer.

An empirical fit describing the variations of the physical ground temperature with time and latitude has been determined from the accumulated measurements of the Cassini Composite Infrared Spectrometer (CIRS) through December 2013 [*Tan et al.*, 2015]. *Janssen et al.* [2016] include a correction factor F_{2cm} to further adjust this relationship to the radiometry data that sample greater than do shorter CIRS wavelengths. This correction is found to be small, and T_{eff} (in K) can be expressed as follows:

$$T_{\text{eff}} = 86.1 + 7.47F_{2cm}\cos(0.0106(\text{lat} - (5.18(t - 2009.61) - 2.98))) \tag{9}$$

where the correction factor F_{2cm} is 0.87 ± 0.05, lat is the latitude in degree, and t is the epoch of observation expressed in year (the vernal corresponds to $t = 2009.61$).

This formula reproduces the 2–4 K equator-to-pole temperature gradient reported in *Janssen et al.* [2009] and the beginning of the warming of the northern hemisphere that has started shortly after the vernal equinox [*Janssen et al.*, 2016]. However, it is important to mention that there is a caveat in using equation (9) as far as the seas are concerned: this law is mainly based on nonmare observations. As a consequence, if the effective temperature of the sea is smaller than that of the surrounding lands, equation (8) with equation (9) will lead to an underestimated emissivity. On the contrary, if the sea is warmer, it will overestimate its emissivity. This question is further discussed in section 4.1. Meanwhile, we note that CIRS data collected during the few close encounters of the northern seas show that the temperature difference between the seas and their surrounding terrains is less than 1 K (D. Jennings, personal communication, 2015).

3.2. Cassini High Spatial Resolution Radiometry Observations of Ligeia Mare

During the first almost 10 years of the mission, from October 2004 to December 2013, Ligeia Mare was observed with high spatial resolution on seven occasions (see Table 1). All these observations were made

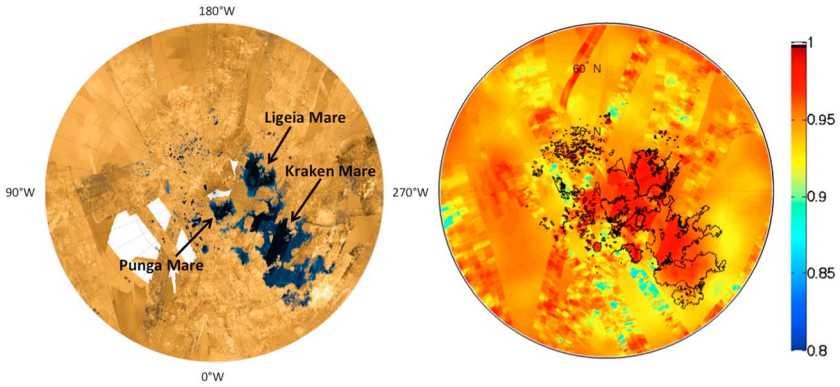

Figure 3. North pole of Titan as seen by the (left) active and (right) passive observations of the Cassini RADAR accumulated from 2004 to February 2014. The radiometry mosaic shows the surface emissivity at 2.2 cm corrected to normal incidence (derived from equation (8)). It is absolutely calibrated to 1% [*Janssen et al*., 2016]. All Ligeia Mare has now been observed by the Cassini radiometer at high spatial resolution (5–50 km). Randy Kirk, a RADAR team member at the U.S. Geological Survey, made the radar mosaics, which use false color to distinguish liquid from dry land and have been cosmetically modified to minimize the appearance of seams.

in the SAR mode of operation of the Cassini RADAR except for one that occurred on 23 May 2013 during the T91 flyby as the instrument was operating as a nadir-looking altimeter. In this paper, particular attention is paid to the data collected during that flyby. Since December 2013, Ligeia Mare has been closely observed two more times, but because the near-polar temperatures may be changing differently than described by equation (9) (derived from CIRS data accumulated through December 2013; see section 3.1), the analysis of these observations must be conducted with caution (see section 4.1). One additional SAR observation of the sea is scheduled before the end of the Cassini Solstice mission, during Titan flyby T126 (22 April 2017).

The global emissivity mosaic of Titan's north pole is displayed in Figure 3. It was obtained from the brightness temperature mosaic using equation (8) assuming that the seas share the same temperature as the lands

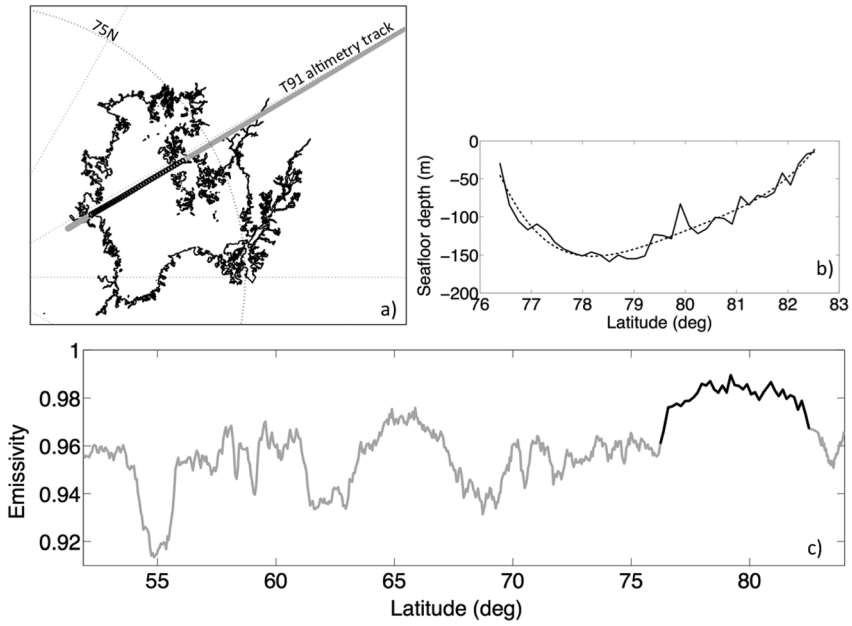

Figure 4. (a) T91 altimetry track over Ligeia Mare. Radiometry footprints that are lying entirely within the sea are shown in black. (b) Bathymetry profile of Ligeia Mare (adapted from *Mastrogiuseppe et al*. [2014]). The dashed line indicates the fourth-order polynomial fitting the depth values. (c) Emissivity profile recorded during the T91 altimetry pass. The emissivity values measured over Ligeia Mare are in black.

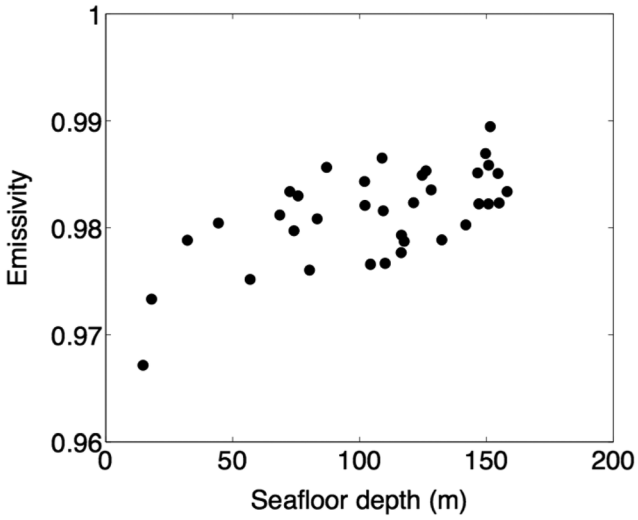

Figure 5. Emissivity at 2.2 cm as measured over Ligeia Mare during the T91 altimetry observation versus the depth of the seafloor derived from active radar data in *Mastrogiuseppe et al.* [2014]. Only the measurements acquired over radiometry footprints that are filled by 99% of Ligeia Mare are considered.

surrounding them. The outlines of the seas were drawn from a mosaic of SAR (synthetic aperture radar), VIMS (visible and infrared mapping spectrometer), and ISS (Imaging Subsystem) images. The seas are, along with the dune fields, the most emissive features on Titan's surface. Their emissivity is exceptionally high, 0.988 ± 0.010 on average (from the first seven observations listed in Table 1), very close to the unity—the emissivity of an ideal black body. The emissivities of the seas are also generally 5–10% greater than that of the surrounding lands (see also Figure 4c). In particular, Ligeia Mare appears as a remarkably radiometrically warm expanse while it is dark on the RADAR backscatter mosaic. As developed later in the paper, this is consistent with the low dielectric constant of liquid hydrocarbons and also implies that the surface of the sea is smooth at the wavelength scale with little or no scattering inside the liquid volume.

The active data collected by the Cassini RADAR during flyby T91 over Ligeia Mare are exceptional because, for the first time, the floor of an extraterrestrial sea was detected [*Mastrogiuseppe et al.*, 2014]. The bathymetry profile constructed from the difference in time of arrival of the surface and bottom echoes displays a maximum depth of ~160 m along the observed transect (see Figure 4b). The emissivity profile acquired concurrently with the active data (i.e., with the same geometry and over the same area of the sea) is shown in Figure 4c. It reaches a maximum around the center of Ligeia Mare and falls off toward the edge. As anticipated from the two-layer model described in section 2 [see also *Lorenz et al.*, 2003, Figure 8], the emissivity profile is correlated with the depth profile, with the most emissive areas being the deepest. Figure 5 further demonstrates the positive correlation between the measured emissivity and local depth of the seafloor. This validates the approach adopted in section 4 that consists in using the two-layer model in order to find the parameter values that best fit the T91 radiometry data. Doing so, new constraints on the composition of not only the liquid but also the seafloor can be inferred.

4. Results and Discussion

4.1. Search for Seasonal Changes and Temperature Difference Between Ligeia Mare and Its Surrounding Lands at the Epoch of T91

The Cassini probe arrived in 2004 just after Saturn's northern winter solstice, and its latest extension, called the Solstice mission, started after the vernal equinox in August 2009 (the beginning of spring in the northern hemisphere and fall in the southern hemisphere) and will continue until a few months past northern summer solstice in May 2017. One of the main scientific objectives of the Cassini Solstice mission is to monitor the changing seasons on Titan. This explains why several recent Cassini flybys over the moon were dedicated to seas: looking for level change, sign of evaporative cooling, or windblown waves. At least two observations hint at possible waves, respectively, on Punga Mare [*Barnes et al.*, 2014] and Ligeia Mare [*Hofgartner et al.*, 2014]. In addition, both RADAR and ISS have observed the disappearance of several smaller lacustrine features in the south polar region between solstice and equinox [*Turtle et al.*, 2009; *Hayes et al.*, 2011]. There may also be evidence that the shorelines of Ontario Lacus have receded during the southern summer [*Turtle et al.*, 2011], but it remains controversial due to the low quality of the initial ISS images [*Cornet et al.*, 2012].

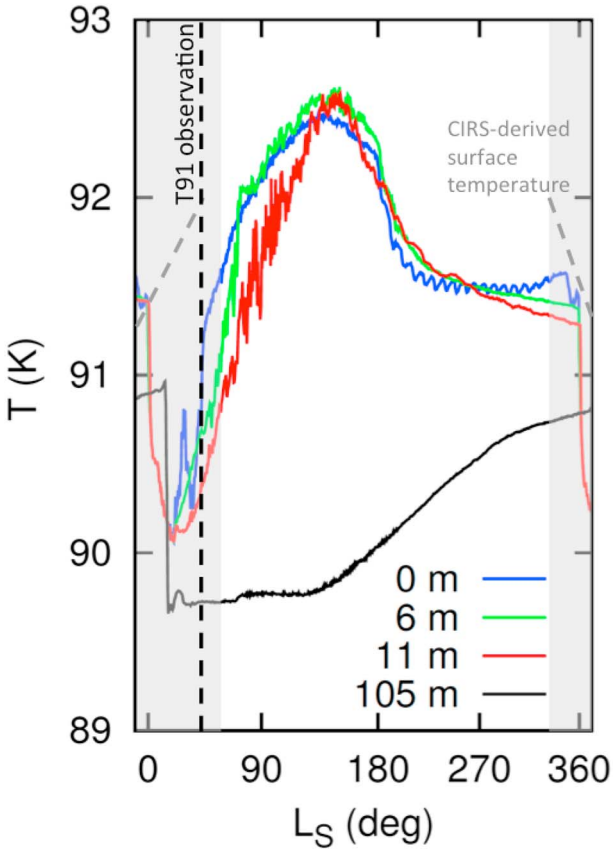

Figure 6. Predicted temperature at different depths (0, 6, 11, and 105 m below the sea surface) in Ligeia Mare as a function of the solar longitude. These curves were obtained using the ocean circulation model described in section 4.1. The gray shaded area indicates the period of observation of Ligeia Mare. The dashed black line indicates the epoch of the T91 altimetry observation ($L_s = 42°$). The dashed gray line displays the surface temperature as derived from CIRS observations (i.e., equation (9) for $F_{2cm} = 1$).

The analysis of radiometry observations collected over Titan's seas can contribute to the search of seasonal changes by, for instance, looking for signs of evaporative cooling. In this section, we search for those signs and discuss the potential temperature difference between Ligeia Mare and its surrounding lands at the epoch of the T91 observation to determine whether we may be overestimating or underestimating its emissivity using equations (8) and (9) (see section 3.1). This discussion is key for the analysis of T91 data conducted in the following section.

4.1.1. Model Predictions

The three-dimensional ocean circulation model for Titan's seas developed by *Tokano and Lorenz* [2015] predicts a drop of the temperature of the sea during the northern spring (see Figure 6). We note that this drop affects the entire liquid column. This might be considered a surprising result—while solar heating indeed warms the sea slightly, the warming of the atmosphere here and elsewhere leads to stronger winds, which in turn cause stronger evaporative cooling. This indirect effect is, in fact, the stronger one—a similar counterintuitive effect can occur on Earth, where evaporation may be enhanced in winter due to stronger winds and dryer air, even though temperatures are lower. Once the sea surface becomes colder than the interior, a convective overturn is predicted which eventually vertically homogenizes the density and reduces the sea temperature at depth [*Tokano*, 2009]. Simulations further show that at any point after the summer solstice, the evaporative cooling is balanced by the increasing insolation.

Figure 6 thus suggests that the general cooling of Ligeia Mare should be effective at the time of the T91 observation. In other words, the effective temperature of the sea should be smaller than that of the surrounding lands and using equation (8) would then lead to an underestimated emissivity value. However, the exact timing of the cooling depends on many unknown factors (*Tokano and Lorenz* [2015] explore the effect of varying turbidity, which influences how deep a column over which the solar heat is deposited, for example) and simulations only really rule out the hypothesis of a sea warmer than its surroundings. As a further argument, liquid having a larger thermal inertia than porous dry solid surface, summer warming is expected to be slower over marine features.

In our study we use a version of the ocean circulation model in which solar heating, methane precipitation, wind stress, and Saturn's tides are simultaneously included. Heat is transported in the sea by advection, turbulent diffusion, and convection. Sources and sinks of heat are imposed at the sea surface, although some in situ solar heating is also assumed to occur inside the sea. The source and sink terms comprise absorption of solar shortwave radiation, net emission of thermal radiation from the sea surface, sensible heat flux between sea surface and air, and latent heat flux associated with methane evaporation from the sea surface. The seasonal cycle is fully accounted for, while the diurnal cycle is neglected. The model

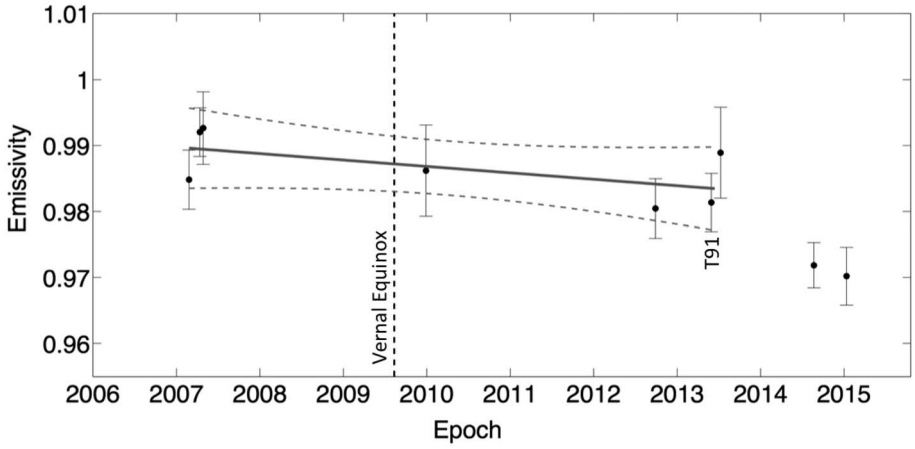

Figure 7. Mean emissivity (corrected to normal incidence) of Ligeia Mare over the course of the Cassini mission through T108 (January 2015). Only radiometry footprints entirely lying in the sea were considered in order to limit the contribution from the nearby shores and large islands. Error bars are measurement standard deviations. Titan passed through the vernal equinox in August 2009 (black dashed line). The best fit linear model (in the least squares sense) for the data collected before December 2013 is plotted in gray. The dashed gray lines demarcate the 95% confidence interval, i.e., the area that has 95% chance of containing the regression line. They show that the radiometry observations cannot discriminate between stable and cooling temperatures. The emissivity values derived from observations acquired after December 2013 are subject to caution because there is no reliable model available for the effective temperature at this epoch (i.e., equation (9) is most probably not valid anymore). Rather than a change of emissivity, they are most likely indicative of the evaporative cooling of the sea or of a general lag in the summer warming of northern polar terrains.

sea has an assumed initial methane mole fraction of 70%, ethane mole fraction of 10%, and nitrogen mole fraction of 20%, but the composition changes in space and time as a consequence of precipitation/evaporation, horizontal, and vertical mixing. Furthermore, the model assumes a sea surface albedo of 0.1, surface bolometric emissivity of 1, and light extinction coefficient of 0.1 m^{-1}. The imposed methane precipitation rate varies with season and latitude, with a global maximum of 4 mm/d assumed at the north pole at summer solstice.

4.1.2. Radiometry Observations Until December 2013

Figure 7 displays the emissivities measured from February 2007 to August 2014 over Ligeia Mare. The (flat) linear regression and its associate interval of confidence corresponding to the data collected between February 2007 and July 2013 cannot discriminate between stable and falling or even slightly increasing temperature. This strongly suggests that Ligeia Mare has not experienced significant net cooling, conservatively less than 2 K—most likely less than 1 K, during this period. We recall that if the temperature variations affect only a thin layer below the surface, then it would be masked by the fact that the radiometer is probing the entire liquid column.

More specifically, if we make the reasonable assumption that the temperature difference between Ligeia Mare and its surrounding lands was minimal at the end of the winter (i.e., in 2007 during the T25, T28, and T29 observations) and that its 2.2 cm emissivity has not changed since then, the relative flatness of the curve in Figure 7 implies that the effective temperature of Ligeia Mare during the T91 observation was still close (±1 K) to that of its surrounding lands and most likely smaller than larger as supported by model predictions. This constraint will serve for the analysis of the T91 data.

4.1.3. Radiometry Observations After December 2013

Figure 7 also shows the emissivities derived from two high-resolution radiometry observations that occurred after December 2013. The corresponding drop in the emissivity confirms that the temporal variations of the effective temperature are not well described by equation (9) for this period. Considering that the emissivity should remain constant, equation (9) overestimates the effective temperature of the sea by about 1 K. This could be indicative of either the evaporative cooling of the sea or of a general lag in the summer warming of the northern polar terrains. CIRS's most recent observations clearly speak in favor of this latter hypothesis [*Jennings et al.*, 2016]. This lagging temperature increase strongly suggests that the northern polar lands are saturated with liquid.

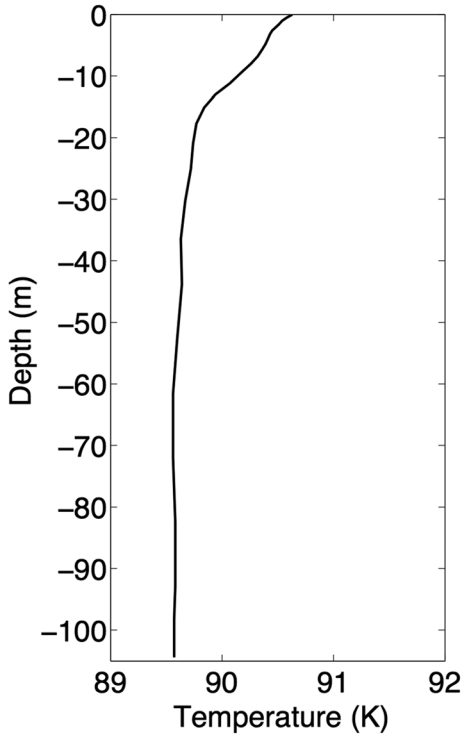

Figure 8. Predicted temperature profile in Ligeia Mare at the time of the T91 altimetry observation ($L_s = 42°$). This curve was obtained using the ocean circulation model described in section 4.1.

4.2. Model Parameter Estimation

Three parameters of the two-layer model applied to Ligeia Mare are readily set: the depth d is known from the bathymetry curve (see section 3.2), the angle of observation θ is zero (nadir-looking geometry), and the RMS surface height σ_{h1} was estimated by *Zebker et al.* [2014] to be 1 mm. We also consider the case of a perfectly smooth sea surface (i.e., $\sigma_{h1} = 0$). In the absence of information, the seafloor is assumed to be smooth at small scale (i.e., $\sigma_{h2} = 0$). Lastly, we treat both the case of an isothermal sea (i.e., $T_1 = T_2$) and that of sea which bottom is cooler than the surface (namely, $T_2 = T_1 - 1$ K) as prompted by the three-dimensional ocean circulation model developed by *Tokano and Lorenz* [2015] which predicts that the temperature of the seafloor of Ligeia Mare was about ~1 K cooler than that of the sea surface in May 2013 (see Figure 8).

We are thus left with three unknown parameters, namely, the dielectric constant of the liquid layer ε_1, its loss tangent $\tan\delta$, and the dielectric constant of the seafloor ε_2. In order to determine them, we fit the emissivity measured during the T91 altimetry pass and associated uncertainties to the model using the Levenberg-Marquardt method [*Levenberg*, 1944; *Marquardt*, 1963; *Press et al.*, 1988] for nonlinear least squares estimation. This approach assumes that the parameters do not vary along the T91 transept. We repeat it for different possible effective temperature differences ΔT between the sea and the surrounding lands, ΔT varying between −1 K and +1 K, and being most likely null or negative (i.e., sea at the same effective temperature or cooler than the lands) as constrained in section 4.1. Model best fit parameters are found by minimizing the reduced chi-square statistics defined as

$$\chi_v^2 = \frac{1}{N-4}\sum_{i=1}^{N}\frac{\left(T_{bi}^{\mathrm{meas}} - T_{bi}^{\mathrm{mod}}\right)^2}{\mathrm{var}\left(T_{bi}^{\mathrm{meas}}\right)} \tag{10}$$

where N is the number of data points ($\nu = N - 3 - 1$ is the number of degrees of freedom), T_{bi}^{meas} are the

Table 2. Model Fitting Results Assuming That the Effective Temperature of Ligeia Mare Does Not Differ From That of Its Surrounding Lands (i.e., $\Delta T = 0$ in Figure 9)[a]

	ε_1			ε_2			$\tan\delta$ ($\times 10^{-5}$)			
	Mean	LCL	UCL	Mean	LCL	UCL	Mean	LCL	UCL	χ_v^{2c}
$T_1 = T_2$, smooth	1.67	1.29	1.98	2.91	2.04	3.79	3.2	1.4	7.5	1.7
$T_1 = T_2$, $\sigma_{h1} = 1$ mm[b]	1.69	1.30	2.00	2.94	2.05	3.84	3.2	1.4	7.5	1.7
$T_2 = T_1 - 1$ K, smooth	1.65	1.21	1.98	2.51	1.71	3.28	3.5	1.6	7.7	1.4
$T_2 = T_1 - 1$ K, $\sigma_{h1} = 1$ mm[b]	1.67	1.21	2.01	2.53	1.71	3.32	3.5	1.6	7.7	1.4

[a]The best fit parameters are reported as well as their lower and upper confidence limits (LCL and UCL) of the 90% confidence interval. The net uncertainty of 1% has been accounted for.
[b]The RMS surface height of the sea surface is derived from active altimetry [*Zebker et al.*, 2014] and divided by 3 before being used as an input in equation (7).
[c]Reduced chi-square as defined by equation (10).

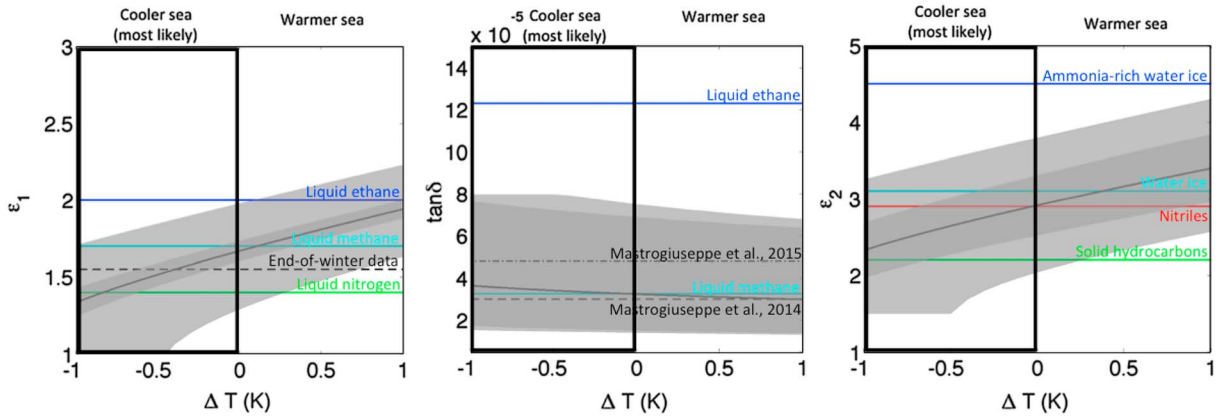

Figure 9. Model fitting results as a function of the temperature difference ΔT (in K) between Ligeia Mare and the surrounding lands for (left) the dielectric constant of the liquid ε_1, (middle) the loss tangent of the liquid tan δ, and (right) the dielectric constant of the seafloor ε_2. These results were obtained assuming a smooth sea surface and an isothermal sea. The associate reduced chi-square values are all ~1.7. The dark gray shaded areas show the upper and lower confidence limits of the 90% confidence interval accounting for the relative error on radiometry measurements. The light gray shaded areas show the upper and lower confidence limits of the 90% confidence interval accounting for both the relative and absolute errors on radiometry measurements. The black rectangles highlight the most likely results (obtained for $\Delta T \leq 0$ K), the hypothesis of the sea warmer than its surrounding being highly implausible as explained in section 4.1. The values of the dielectric constant and loss tangent of materials relevant to Titan's surface as well as results from other observations are indicated for comparison.

measured 2.2 cm brightness temperatures, T_{bi}^{mod} are the brightness temperatures modeled as described in section 2, and $\mathrm{var}\left(T_{bi}^{\mathrm{meas}}\right)$ is the variance, related to the measurement systematic errors. As shown by *Janssen et al.* [2016], the brightness measurements exhibit normally distributed errors, enabling the use of the χ_ν^2 minimization as a maximum likelihood estimator for model parameters. The standard deviation of the measurements acquired within one same pass is estimated to be less than 0.5% (see section 3.1). The parameter values are estimated along with their 90% confidence interval bounds. Lastly, we account for the net uncertainty of 1% on the measured emissivities to estimate the even more conservative upper and lower confidence limits reported in Table 2.

Table 2 summarizes the results of the parameter estimation assuming a smooth and a slightly rough sea surface, either with a constant temperature profile or with a seafloor 1 K cooler than the liquid layer, assuming that the effective temperature of Ligeia Mare does not differ from that of its surrounding lands (i.e., $\Delta T = 0$ K). Given the limitations of the model proposed by *Choudhury et al.* [1979] (see section 2), the results obtained in the rough cases are for information purposes only. Anyhow, they only slightly differ from those obtained in the smooth cases. Figure 9 displays the inferred parameters as a function of the temperature difference ΔT between the sea and the land for an isothermal sea with a smooth surface. The most likely results are obtained for $\Delta T \leq 0$, taking the hypothesis that the sea can be warmer than its surroundings to be highly implausible as explained in section 4.1. These results are discussed below.

4.3. Composition of the Sea Liquid

The inferred range of values for the dielectric constant of the liquid is $\leq 1.67 \pm 0.30$ (see Figure 9). This result does not vary significantly with the sea surface roughness (see Table 2) and is further supported by the high emissivity values recorded during the SAR-radiometry observations of Ligeia Mare (see Table 1). This is especially true at the end of the winter, when the temperature difference between the sea and the lands was most probably minimum and the sea emissivity was not underestimated or overestimated. An estimate of the dielectric constant of the column of material probed by the radiometer ε can be obtained from Kirchhoff's law of thermal radiation which relates the emissivity at normal incidence (i.e., for $\theta = 0°$) of a smooth surface to its specular reflectivity Γ through $e = 1 - \Gamma$. This law further implies

$$\varepsilon = \left(\frac{2 - e + 2\sqrt{1 - e}}{e}\right)^2 \tag{11}$$

An average emissivity at normal incidence of 0.988 ± 0.010 (see section 3.2) thus corresponds to a dielectric constant of 1.55 ± 0.25. If the surface displays subwavelength features, ε can be estimated using the following formula (obtained from Kirchhoff's law of thermal radiation substituting $f\Gamma$ to Γ):

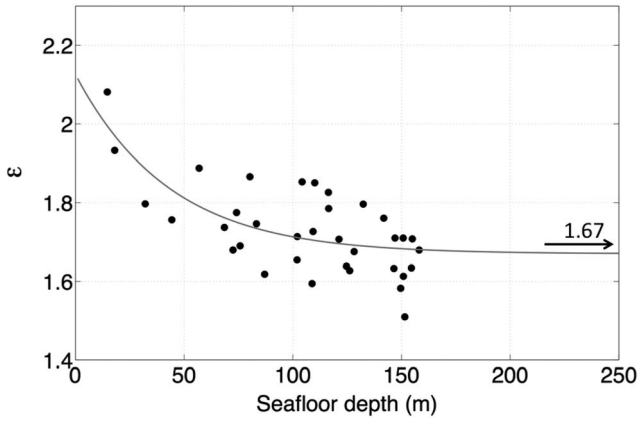

Figure 10. Bulk dielectric constant of the column of material sensed by the Cassini radiometer during the T91 altimetry pass as a function of the seafloor depth inferred from radar active data. The gray line displays the best fit model (in the smooth case assuming $\Delta T = 0$ K) as derived in section 4.2.

$$\varepsilon = \left(\frac{f + 1 - e + 2\sqrt{f}\sqrt{1-e}}{e + f - 1} \right)^2 \tag{12}$$

where f is a surface roughness factor (f is equal to 1 for a smooth surface hence equation (11)). Using f as defined by equation (7) and assuming a RMS surface height of 1 mm divided by 3, we find 1.57 ± 0.25.

We emphasize that the dielectric constant inferred here, in addition to contribution from the sea bottom, may include contribution from the more reflective nearby shores and embedded small islands. The value 1.8 (i.e., 1.55 + 0.25) must therefore be regarded as a strict upper bound for the dielectric constant of the liquid of the Ligeia Mare. Due to the contribution of the seafloor at shallow depths, the best estimate of the dielectric constant of the liquid can be obtained considering only the most central and deepest regions of the seas (i.e., where the thermal emission from the shore and bottom is minimum). In fact, when applying equation (11) or (12) to the emissivity values measured during T91, we find that the effective dielectric constant decreases with depth, asymptotically trending toward the dielectric constant of the liquid inferred in section 4.2 (see Figure 10).

Such a low best fit dielectric constant not only is consistent with liquid hydrocarbons but also suggests that the composition of Ligeia Mare is dominated by liquid methane rather than liquid ethane (see Figure 9 and Table 3). Recent laboratory measurements [*Mitchell et al*., 2015] have confirmed previous work (see a review

Table 3. Dielectric Constants and Loss Tangents of Materials Relevant to Titan's Surface at ~13.78 GHz (the Operating Frequency of the Cassini RADAR)[a]

Materials	Dielectric Constant ε	Loss Tangent $\tan\delta$	References/Comments
Liquid nitrogen	~1.40	$5.2 \pm 1.4 \cdot 10^{-5}$	ε is extrapolated from *Jiang and Zhang*'s [2011] results obtained at 1 MHz and lower temperatures. *Paillou et al*. [2008] report a dielectric constant of 1.45 at 77 K and 13 GHz. $\tan\delta$ was obtained for liquid nitrogen at 77 K by *Smith et al*. [1990] at 15 GHz. *Paillou et al*. [2008] report a higher loss tangent, closer to that of liquid ethane.
Liquid methane	1.73	$3.26 \pm 1.01 \cdot 10^{-5}$	Values here are from *Mitchell et al*. [2015]. Extrapolating *Singh and Miller*'s [1978] results at 92 K, pure methane has a dielectric constant of 1.67, suggesting that values from *Mitchell et al*. [2015] may be high. Similarly, *Leese et al*. [2012] give near-DC values at ~92 K of 1.675 and 1.94 for liquid methane and ethane, respectively.
Liquid ethane	2.00	$1.23 \pm 0.17 \cdot 10^{-4}$	
Methane-nitrogen mixtures	90%–10%: 1.64 75%–25%: 1.60 50%–50%: 1.52	Not available	Extrapolating *Singh and Miller*'s [1978] results at 92 K. Reproducibility stated as 0.03, but relative precision is likely rather better than this.
Solid hydrocarbons	2–2.4	$10^{-4} - 10^{-2}$	From *Paillou et al*. [2008], obtained at 77 K and 10 GHz. The range of values of ε reflects different compositions: solid heptane has a dielectric constant of ~2, while solid benzene has a dielectric constant of ~2.4 (see also Appendix A). The dielectric constant of tholin powder can be lower than 2 if poorly compacted.
Nitriles	2.85–2.95	Not available but likely $>10^{-2}$	Measured on frozen acrylonitrile (C_2H_3CN) and acetonitrile (CH_3CN) as described in Appendix A.
Water ice	3.1	$\sim 10^{-4}$	From *Paillou et al*. [2008], obtained at 77 K and 10 GHz. *Lamb and Turney* [1949] give 3.17 and 0.2×10^{-4} at ~90 K and 24 GHz.
Ammonia-rich water ice	~4.5	$10^{-3} - 10^{-2}$	From *Paillou et al*. [2008] obtained at 77 K and 10 GHz. Also, ~4.5 from *Lorenz* [1998] obtained at 83 K and 100 Hz, 4.7 in this work (see Appendix A). Both were obtained for ~30% of ammonia.

[a]Uncertainties on dielectric constants are likely ~0.02 unless otherwise stated.

in *Lorenz et al*. [2003, Table 1]) showing that pure liquid methane has a significantly lower dielectric constant (~1.7) than pure liquid ethane (~2). However, we note that the presence of nitrogen, which has a very low dielectric constant (~1.4; see Table 3), would allow some ethane in the liquid mixture and still be consistent with radiometry results and their associated uncertainties (i.e., nitrogen's low dielectric constant can offset that of ethane). We recall that nitrogen dominates the composition of Titan's atmosphere (~95%) and is soluble in methane. The solubility in ethane is much lower (although not quite as low as quoted in *Battino et al*. [1984], which contains a typographical error: the second term in equation 40 of *Battino et al*. [1984] should be a plus sign, not minus, and the corresponding Table 34 was computed incorrectly (G. A. Landis, personal communication, 2014; R. Battino, personal communication, 2014)). Recent experiments have shown that a liquid of pure methane can dissolve up to ~30% of nitrogen while no observable dissolution occurred in pure ethane liquid [*Chevrier et al*., 2015]. Hence, a single-phase nitrogen-ethane mixture, while in principle compatible with the dielectric constant from radiometry, is not thermodynamically permitted. The radiometry observations allow a pure methane composition but do not allow much ethane without also requiring nitrogen to offset it. Further laboratory experiments on the amount of nitrogen dissolving in a mixture methane-ethane would greatly help to place an upper bound on the concentration of ethane.

The very low inferred range of values for the liquid loss tangent ($< 3.6^{+4.3}_{-2.1} \times 10^{-5}$; see Table 2 and Figure 9) offers a further, and maybe stronger, argument for a methane-dominated composition. It is very close to the value measured in laboratory by *Mitchell et al*. [2015] which found liquid methane to have ~5 times smaller loss tangent than liquid ethane (see Table 3). Nitrogen has a loss tangent somewhat close to that of pure methane. Though less constraining, our result agrees very well with both *Mastrogiuseppe et al*. [2014] (submitted manuscript, 2016) results ($(3.0 \pm 1.0) \times 10^{-5}$ and $(4.8 \pm 1.0) \times 10^{-5}$, respectively). Based on the former, *Mitchell et al*. [2015] estimate 20% in volume to be a reasonable upper limit for the ethane concentration in Ligeia Mare. Also using the Lorentz-Lorenz mixing model [e.g., *Bosch et al*., 2000], assuming a binary mixture, and using the best fit dielectric values from the laboratory measurements reported in Table 3, we find that within 90% confidence, our results are consistent with a range of compositions ranging from pure methane to a mixture of methane with 50% of ethane.

Regardless, both active and passive RADAR observations point to the remarkable transparency of Ligeia Mare liquid at microwaves and strongly suggest that the sea has no or few suspended particles. A significantly higher loss tangent was inferred for the nearshore (within a few kilometers) region of Ontario Lacus (9.2×10^{-4}) [*Hayes et al*., 2010], perhaps suggesting the presence of absorbing floating or suspended solutes in the shallow sloping nearshore region of the southern lake or perhaps a different hydrocarbon composition with a higher abundance of absorptive polar hydrocarbons or nitriles.

Possible implications of a methane-dominated composition of Ligeia Mare are discussed in *Mitchell et al*. [2015] and Mastrogiuseppe et al. (submitted manuscript, 2016). We add few thoughts here. First, a methane-rich composition would imply that thermodynamical equilibrium state as predicted by *Cordier et al*. [2009, 2013a] does not apply (otherwise the sea would be dominated by ethane which is much less volatile than both methane and nitrogen at Titan's surface conditions). However, new calculations using updated equations of state show that on the long term, surface liquids at polar latitudes, unlike surface liquids at equatorial regions, should be dominated by methane [*Tan et al*., 2013].

Second, there are two distinct ways of obtaining a methane-dominated sea composition in the present epoch when ethane is predicted to be abundant on the surface as the primary product of Titan's stratospheric photochemistry [*Lavvas et al*., 2008; *Krasnopolsky*, 2009]. One is origin and replenishment from fresh rainfall. Indeed, although some calculations suggest that ethane could be present too in the form of liquid or frost [*Graves et al*., 2008; *Dalba et al*., 2012], rain droplets on Titan are predominately composed of methane [*Niemann et al*., 2010]. Alternatively, ethane may be regularly removed from the sea. Less volatile and denser ethane could be trapped in subsurface reservoirs assuming a porous regolith as suggested by *Hayes et al*. [2008], followed by seasonal drying then followed by gentle layering of the precipitated methane onto the ethane surface as proposed by *Stevenson and Potter* [1986]. *Choukroun and Sotin* [2012] propose another possible mechanism of sequestration of the ethane in the subsurface based on the idea that ethane would substitute for methane while percolating in liquid form in clathrate layers potentially existing in the polar regions. *Mousis et al*. [2015] recently predict that if the seas are in contact with these hypothetical subsurface springs and if their initial composition contains less than 75% of ethane, then they should be methane rich. Furthermore, even if the sea is initially ethane

rich, one could argue that if the bottom of Ligeia Mare is somehow connected with this layer of clathrate hydrates, then ethane will progressively substitute for methane in the subsea crust thus resulting in the enrichment in methane of the sea with time.

Were one of these scenarios to be proven, all northern seas could share the same methane-dominated composition (provided that the same communication mechanism is at work). Alternatively, *Lorenz* [2014] proposes another process to eliminate ethane from Ligeia Mare: somewhat analogous to salts in terrestrial waters, ethane, with other solutes, could be flushed out by fresh rainfall from Ligeia Mare into Kraken Mare via the narrow channels that connect the two seas (see Figure 3), much as rain on Earth leads to the Baltic Sea being less salty than the Atlantic into which it drains. This "flushing" scenario relies on the idea that Titan's hydrological cycle introduces more "fresh" precipitation at the highest latitudes (Ligeia Mare being farther north than Kraken Mare) and could be tested looking for the signature of a latitudinal gradient in the methane concentration. So far, radiometry observations do not support any obvious compositional difference between Ligeia Mare and Kraken Mare but this deserves to be investigated further.

4.4. Composition of the Seafloor

Though the error bar is conservative, our result on the dielectric constant of the seafloor, namely, $\varepsilon_2 < 2.9^{+0.9}_{-0.9}$, does not put a strong constraint on the composition of the seafloor. We note that if the seafloor is not smooth at small scale as assumed (i.e., if $\sigma_{h2} \neq 0$), then a slightly higher dielectric constant is required to best fit the data. The contrary will be true if the seafloor is cooler than predicted by our sea circulation model. We recall that a value of 2.3 ± 0.25 was found for the dielectric constant of the shores of Ligeia Mare [*Zebker et al*., 2014] also using the T91 data set (see also Figure 4c: the emissivity of the lands around the sea is ~0.96, consistent with a dielectric constant of ~2.25 using equation (11)). Given the relative precision of the radiometer within a single data set (see section 3.1), we estimate that the relative error on ε_2 is ~0.3 (versus an absolute error of ~0.9). We discuss the implications of this result for the composition of the seafloor below.

Titan's deep crust is thought to be made of water ice in its solid form or as clathrate hydrates, in which the guest species is primarily methane, ethane, or both, with any ammonia in the underlying liquid water [e.g., *Tobie et al*., 2005, 2006]. Water ice has a dielectric constant of 3.1, and that can be up to 4.5 if it is ammonia rich (see Table 3). To first order, clathrate hydrates have dielectric properties analogous to that of porous water ice, i.e., a dielectric constant approaching 2 [*Sloan and Koh*, 2008]. An icy subsea crust would explain the upper values obtained for ε_2. Further, if both the shores and the seafloor of Ligeia are composed of water ice with some porosity, their difference in terms of dielectric constant could be simply explained by the fact that the pores are filled with air on the shores while they are saturated with liquid on the seafloor. However, we much favor a scenario wherein both the seafloor and the shores are covered by organic materials. As a matter of fact, outside the seas on the dry surface, there is little water ice obviously exposed on Titan. Detailed mapping of Titan's surface reveals that most of the surface areas examined seem to be covered by a sedimentary layer of solid organics [*Janssen et al*., 2016; *Lopes et al*., 2016; M. J. Malaska et al., Geomorphological map of the Afekan crater region, Titan: Terrain relationships in the equatorial and mid-latitude regions, submitted to *Icarus*, 2015], likely originating from methane photolysis in the atmosphere.

The complex atmospheric photochemistry on Titan produces a wealth of organic molecules that are eventually deposited at the surface [*Lavvas et al*., 2008; *Krasnopolsky*, 2009]. Among these compounds, some of them will dissolve in the liquid composition contained in the seas. Laboratory experiments have showed that even at Titan's cryogenic temperatures, dissolution will occur rapidly [*Malaska and Hodyss*, 2014]. If the amount of material deposited in the sea is higher than the amount that can be contained in sea solution, then saturation of the fluids will occur [*Raulin*, 1987; *Cordier et al*., 2009]. The excess should then form a sludge layer at the bottom of the seas, as predicted by laboratory experiments on the solubilities of aromatic molecules in cryogenic liquid ethane [*Lorenz and Lunine*, 1996; *Malaska and Hodyss*, 2014].

Solid materials can be brought to the sea not only by direct air fall but also by fluvial action or rain washing of the surrounding terrains and, in particular, of the evaporite deposits ringing Ligeia Mare [*Barnes et al*., 2011; *Cordier et al*., 2013b] as illustrated by Figure 11. Materials delivered from the surface into the seas will significantly decrease the time to sea saturation. For most organic molecules, the solubility in liquid methane is significantly lower than that in liquid ethane [*Raulin*, 1987; *Glein and Shock*, 2013; *Cornet et al*., 2015]. Thus, the

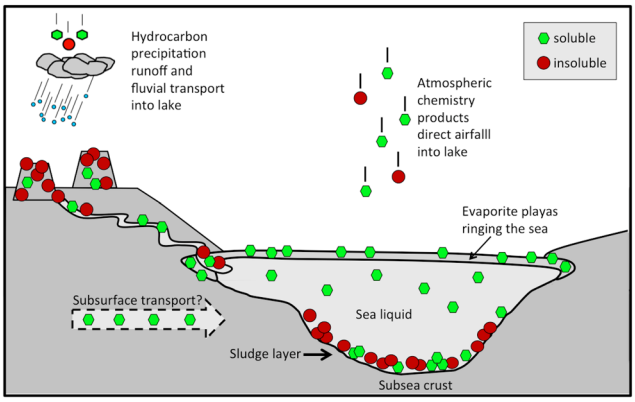

Figure 11. Diagram showing processes bringing solid material on the seafloor of seas and lakes.

sludge layer should be thicker in a methane-dominated sea compared to an ethane-dominated sea given the same amount of material input.

Once deposited in the sea bottom, any material not subjected to dissolution will become part of the sludge layer and, if the material has appreciable cohesion, will remain there. More specifically, *Tokano and Lorenz* [2015] report that bottom currents in Ligeia Mare predicted by the circulation model frequently exceed 2 mm/s, enough to suspend sand-sized (100 μm) particles in liquid hydrocarbons in Titan gravity [*Burr et al*., 2006]. Thus, loosely bound fine-grained sediments may be frequently mobilized and could in principle be washed out of the sea.

Candidates for the composition of the solid substrate of Titan's seafloor are therefore based on a combination of species abundance and solubility. Based on photochemical models [*Lavvas et al*., 2008; *Krasnopolsky*, 2009], acetylene (C_2H_2) and hydrogen cyanide (HCN) are produced in large amount in the atmosphere. As such, they may saturate the seas even though their solubilities in liquid hydrocarbons is relatively high [*Raulin*, 1987; *Cordier et al*., 2009]. Due to their abundance, they should also dominate the composition of evaporites [*Cordier et al*., 2013b]. Furthermore, deposits of acetylene and HCN have the potential to be chemical feedstocks for the formation of insoluble polymers, although at Titan's low temperatures it is not clear if surface chemistry will play a dominant role. In the *Krasnopolsky* [2009] atmospheric model, polymeric materials make up a significant fraction of the downward surface flux deposited on the surface. Likely insoluble compounds include haze particles previously mentioned (thought to be similar to laboratory tholins), polyaromatic hydrocarbons, and highly polar molecules resulting from hydrolysis in impact melts [*Neish et al*., 2009], and water ice (atmospheric infall from exogenic sources).

Other materials are predicted to be produced in much lesser quantities in the atmospheric chemistry models compared to acetylene and HCN but are also thought to be significantly less soluble. These include nitriles such as acetonitrile (CH_3CN), acrylonitrile (C_2H_3CN), and cyanoacetylene (HC_3N) as well as benzene (C_6H_6) that has been detected by VIMS at the surface of Titan [*Clark et al*., 2010]. The solubility of benzene has been measured in both liquid methane and ethane at cryogenic temperature in Titan conditions and found to be low, on the order of 10 mg/L and 100 times lower than this concentration for methane [*Diez-y-Riega et al*., 2014; *Malaska and Hodyss*, 2014]. For a 100 m deep ethane sea, *Malaska and Hodyss* [2014] estimated that saturation from benzene air fall alone, no fluvial transport required, would be reached on the order of 100 Myr. It should be even faster for a methane-rich sea.

All the compounds previously mentioned have a bulk dielectric constant in the range 2–3 (see Table 3) and could thus well explain the inferred range of values for the dielectric constant of the seafloor. If the dielectric constant of the seafloor was proven to be larger than that in the shores of Ligeia Mare (as suggested by the inferred mean values in Table 2), it would suggest that the depositional organic layer at the bottom of Ligeia Mare is more compacted and/or more nitrile rich than that on the shores (see Table 3).

4.5. Low-Resolution Bathymetry Map

Using the two-layer model with the inferred values of ε_1, ε_2, and $\tan\delta$ as inputs and assuming that the compositions of the liquid and of the seafloor are uniform across the sea, the emissivity map of Ligeia Mare can be converted into a low-resolution bathymetry map. However, given the fact that the emissivity is expected to vary by at most 1% with depth (see section 2 and Figure 2) which is the order of magnitude of the systematic error in the emissivity mosaic (see section 3.1), we chose to limit the sources of measurement deviation by building this map using only data collected closely in time, with low or moderate emission angles and with a relatively stable parallel polarization. This left us with only two data sets: T28 and T29

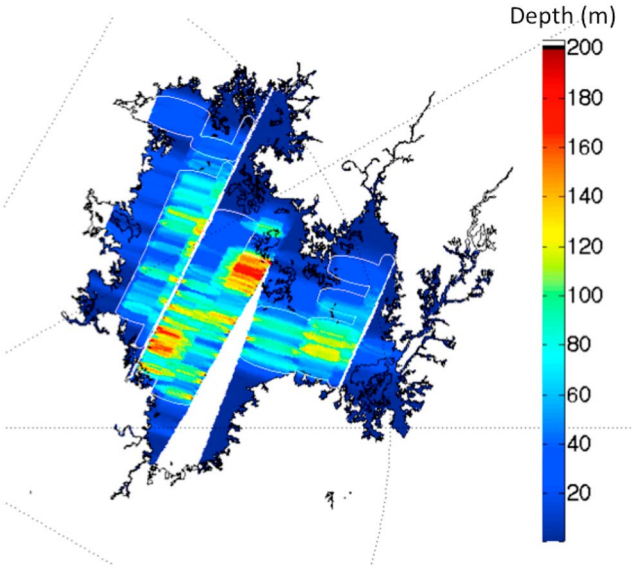

Figure 12. Bathymetry map of Ligeia Mare inferred from two radiometry observations at closest approach of the sea, namely, T28 and T29. The resolution of this map is that of the radiometer, i.e., 12–15 km and 15–79 km, respectively, along and across the T28 and T29 swaths (see Table 1). Data acquired in areas outside the white line are likely to be contaminated by the thermal emission from nearby shores and/or islands because the corresponding radiometry footprints are not filled with 100% of sea; the average depth is underestimated here.

(see Table 1). The resulting map is shown in Figure 12. It was obtained using the best fit mean values inferred for the case of an isothermal smooth sea (first case in Table 2), and it was absolutely calibrated using the T91 bathymetry/emissivity profile.

Despite the limited data set we considered, this map must be taken with caution and mainly offers a qualitative indication of the variation of the seafloor depth across Ligeia Mare at the resolution of the Cassini radiometer (12–15 km and 15–79 km, respectively, along and across the T28 and T29 swaths; see Table 1). The depth of sea bottom probably may vary significantly within each radiometry footprint; the inferred bathymetry map provides an average depth. The largest depths are thus not likely to be captured unless they extend over an area comparable in size with the footprint. We also emphasize that the depths inferred outside the white contour in Figure 12 are underestimated because the radiometry measurements there include contribution from the more emissive shores and/or nearby islands.

Nevertheless, Figure 12 contains some information. First, it reveals that the central part, and more specifically the north central part of the sea, is most probably the deepest section of Ligeia Mare. In this area, the depth of the seafloor likely exceeds 200 m, consistent with the maximum depths found in the high-resolution bathymetry map reported in *Hayes* [2016] using the SAR active observations of Ligeia Mare. Second, this map can be used to provide a lower bound for the volume of liquid in the sea. According to the radiometry-derived bathymetry, the volume is $>5000\,km^3$ considering all available pixels (that cover 87% of Ligeia Mare's plan view surface) and $>7000\,km^3$ if we assume that invalid pixels (i.e., missing pixels and pixels outside the white contour in Figure 12) have depths equal to the average depth, namely, ~50 m. This is consistent with the estimate of 14,000 km^3 reported by *Hayes* [2016], which is equivalent to 55 times the volume of all proven natural gas reserves on Earth.

5. Conclusion

In this paper, we have shown that radiometry observations of Titan's surface can provide valuable constraints on the composition of the seas and lakes. Our results on Ligeia Mare add to the confidence of the results obtained in the active mode of the Cassini RADAR and in particular to the loss tangent found for the liquid contained in the sea [*Mastrogiuseppe et al*., 2014] (submitted manuscript, 2015). We emphasize that our result on the loss tangent is independent from that of the active radar because the only information we use from the radar is the bathymetry profile, which does not vary with the loss tangent and only slightly with the dielectric constant. Both passive and active observations point to a composition largely dominated by methane [*Mitchell et al*., 2015]. More definitive and detailed conclusions on the sea composition now await experimental study of, for instance, nitrogen dissolution in a methane-ethane mixture under cryogenic conditions. Measuring the microwave thermal emission of Ligeia Mare also allowed us to provide the first estimation of the dielectric constant of a seafloor, possibly revealing a small but significant difference with that of the shores.

Recently, altimetry profiles were obtained for the two other seas of Titan, namely, Kraken Mare and Punga Mare. In both cases, portions of the altimetry track exhibited double-peaked echoes, indicating that the seafloor was

observed. The active data are currently being analyzed and a similar analysis to the one described herein can be applied to the concurrent radiometry data acquired over these seas. This analysis may reveal compositional differences between the seas and help in understanding their formation and dynamics. In addition to regional differences, the Cassini radiometer may soon bring evidence of seasonal changes on the seas in the form of evaporative cooling. So far, they have revealed a possible general lag in the summer warming of the northern polar terrains which, if confirmed by thermal IR observations, would be the first strong indication that the polar lands are saturated with liquid.

There has been considerable recent interest in future in situ exploration of Titan's seas from floating capsules [e.g., *Stofan et al*., 2013; *Mitri et al*., 2014]: by drifting in currents and winds [*Lorenz*, 2015a], such capsules could traverse Ligeia Mare and measure a profile of the depth and bottom characteristics with sonar at much higher resolution than Cassini. The Huygens probe carried an echo sounder, and detailed sonar modeling in Titan liquids was performed in support of the Titan Mare Explorer (TiME) mission proposal [*Arvelo and Lorenz*, 2013]: such measurements can usefully complement microwave observations from Cassini. The analysis here, suggesting a compacted seabed on Ligeia, indicates that the acoustic reflectivity of the seafloor will yield strong sonar echoes. The modeling showed that the temperature structure of Titan's seas has, as on Earth, important implications for the propagation of sound, for example, that ducting of sound is possible. Thus, a better understanding of the seasonal evolution of temperatures from radiometry observations such as those described in this paper will improve assessment of what such future in situ measurements might be able to achieve. Looking further ahead, there are studies underway [e.g., *Lorenz*, 2015b] on submersible vehicles that might be able to study the seabed on Titan directly and provide direct measurement of the thermal structure—inaccessible to microwave remote sensing by Cassini—of Titan's intriguing lakes and seas.

Appendix A: Dielectric Properties of Possible Sediments/Evaporites

We employed a large parallel-plate capacitor used in previous experiments [*Lorenz*, 1998; *Lorenz and Shandera*, 2001] with a handheld capacitance (LCR) meter which makes a near-DC measurement (nominally ~100 Hz). In general, organics at low temperature have relatively little variation in the real part of the dielectric constant with frequency, so the measurements here are broadly applicable to microwave remote sensing (a possible exception are the nitriles, which may have some frequency dependence near molecular transitions).

The measured capacitance has a value that linearly relates to the dielectric constant ε of the material filling the gap between the plates—$0.6 + 0.5\varepsilon$ nF. The 0.6 offset is due to parasitic capacitance by nylon washers used to space the 12 plates held under compression by nylon bolts and due to cabling. The large area of the capacitor means that fringing effects are minimal (less than a few percent). The capacitor is placed in a polyethylene freezer bag wrapped with tape to keep taut; the bag is filled with the liquid under test and immersed in a Dewar of liquid nitrogen until the temperature (monitored with a thermocouple on an outer plate) becomes constant at 83 K. All measurements were made between −170° and −190°C (83–103 K): in some cases measurements were made spanning this range, and no significant variation in dielectric properties was noted.

We reproduced the known result for water ice (3.1) and found a value of 4.67 for frozen ammonia solution (27–30%) in water, in good agreement with the determination of 4.5 by *Lorenz* [1998]. Frozen benzene prepared by this procedure has a dielectric constant of 2.45.

New results are the dielectric constant for nitriles, which are somewhat higher than hydrocarbons—frozen acrylonitrile and acetonitrile have $\varepsilon = 2.85$–2.95. Although unlikely as a dominant Titan constituent, methanol is present in comets and we measured a dielectric constant of 3.52; ethanol was slightly lower at 3.42. Errors in the absolute dielectric constant are estimated at ~0.05.

Acknowledgments

We wish to thank the Cassini Mission Team and especially the Radar Science Team for continuing to deliver invaluable science data. A. Le Gall is supported by a chair of the French Space Agency CNES/UVSQ (Université Versailles Saint Quentin). J.I.L. benefits of a NASA contract for IDS investigations. A.G.H. and M.M.'s contributions to this work were support by NASA Early Career Fellowship NNX14AJ57G. The radiometry data used in this paper will be soon available on PDS (Planetary Data System) as SBDRs (Short Burst Data Records, i.e., instrument telemetry and calibrated science data in burst order) at the following link: http://pds-imaging.jpl.nasa.gov/volumes/radar.html. We would like to thank D. Jennings for discussions about the measurements and calibration of the CIRS surface temperature measurements over the span of our observations and for providing results in advance of publication that were essential in the present paper. We are also grateful to J. Barnes, W. Fa and an anonymous reviewer for their thoughtful comments that greatly help improving this manuscript.

References

Arvelo, K., and R. D. Lorenz (2013), Plumbing the depths of Ligeia: Considerations for acoustic depth sounding in Titan's hydrocarbon seas, *J. Acoust. Soc. Am.*, *134*, 4335–4351.

Barnes, J. W., et al. (2009), Shoreline features of Titan's Ontario Lacus from Cassini/VIMS observations, *Icarus*, *201*, 217–225, doi:10.1016/j.icarus.2008.12.028.

Barnes, J. W., et al. (2011), Organic sedimentary deposits in Titan's dry lakebeds: Probable evaporate, *Icarus*, *216*, 136–140, doi:10.1016/j.icarus.2011.08.022.

Barnes, J. W., C. Sotin, J. M. Soderblom, R. H. Brown, A. G. Hayes, M. Donelan, S. Rodriguez, S. Le Mouelic, K. H. Baines, and T. McCord (2014), Cassini/VIMS observes rough surfaces on Titan's Punga Mare in specular reflection, *Planet. Sci.*, *3*, 3.

Battino, R., T. R. Rettich, and T. Tominaga (1984), The solubility of nitrogen and air liquid, *J. Phys. Chem. Ref. Data*, *13–2*, 563–600.

Bosch, S., J. Ferré-Borrull, N. Leinfellner, and A. Canillas (2000), Effective dielectric function of mixtures of three of more materials: A numerical procedure for computations, *Surf. Sci.*, *453*, 9–17.

Brown, R. H., L. A. Soderblom, J. M. Soderblom, R. N. Clark, R. Jaumann, J. W. Barnes, C. Sotin, B. Buratti, K. H. Baines, and P. D. Nicholson (2008), The identification of liquid ethane in Titan's Ontario Lacus, *Nature*, *454*, 607–610.

Burr, D. M., J. P. Emery, R. D. Lorenz, G. C. Collins, and P. A. Carling (2006), Sediment transport by liquid surficial flow: Application to Titan, *Icarus*, *181*, 235–242.

Chevrier, V. F., A. Luspay-Kuti, and S. Singh (2015), Experimental study of nitrogen dissolution in methane-ethane mixtures under Titan surface conditions, Abstract 2763 presented at 46th Lunar and Planetary Science Conference.

Choudhury, B. J., T. J. Schmugge, R. W. Newton, and A. T. C. Chang (1979), Effect of surface roughness on microwave emission of soils, *J. Geophys. Res.*, *84*, 5699–5706, doi:10.1029/JC084iC09p05699.

Choukroun, M., and C. Sotin (2012), Is Titan's shape caused by its meteorology and carbon cycle?, *Geophys. Res. Lett.*, *39*, L04201, doi:10.1029/2011GL050747.

Clark, R. N., et al. (2010), Detection and mapping of hydrocarbon deposits on Titan, *J. Geophys. Res.*, *115*, E10005, doi:10.1029/2009JE003369.

Cordier, D., O. Mousis, J. I. Lunine, P. Lavvas, and V. Vuitton (2009), An estimate of the chemical composition of Titan's lakes, *Astrophys. J.*, *707*, L128–L131, doi:10.1088/0004-637X/707/2/L128.

Cordier, D., O. Mousis, J. I. Lunine, P. Lavvas, and V. Vuitton (2013a), Erratum: "An estimate of the chemical composition of Titan's lakes", *Astrophys. J.*, *768*, L23.

Cordier, D., J. W. Barnes, and A. G. Ferreira (2013b), On the chemical composition of Titan's dry lakes, *Icarus*, *226*, 1431–1437, doi:10.1016/j.icarus.2013.07.026.

Cornet, T., et al. (2012), Geomorphological significance of Ontario Lacus on Titan: Integrated interpretation of Cassini VIMS, ISS and RADAR data and comparison with the Etosha Pan (Namibia), *Icarus*, *218*, 788–806.

Cornet, T., D. Cordier, T. Le Bahers, O. Bourgeois, C. Fleurant, S. Le Mouélic, and N. Altobelli (2015), Dissolution on Titan and Earth: Towards the age of Titan's karstic landscapes, *J. Geophys. Res. Planets*, *120*, 1044–1074, doi:10.1002/2014JE004738.

Dalba, P. A., B. J. Buratti, R. H. Brown, J. W. Barnes, K. H. Baines, C. Sotin, R. N. Clark, K. J. Lawrence, and P. D. Nicholson (2012), Cassini VIMS observations show ethane is present in Titan's rainfall, *AstroPhys. J. Lett.*, *761*, L24, doi:10.1088/2041-8205/761/2/L24.

Diez-y-Riega, H., D. Camejo, A. E. Rodriguez, and C. E. Manzanares (2014), Unsaturated hydrocarbons in the lakes of Titan: Benzene solubility in liquid ethane and methane at cryogenic temperatures, *Planet. Space Sci.*, *99*, 28–35, doi:10.1016/j.pss.2014.05.003.

Elachi, C., et al. (2004), RADAR: The Cassini Titan Radar Mapper, *Space Sci. Rev.*, *115*, 71–110.

Glein, C. R., and E. L. Shock (2013), A geochemical model of non-ideal solutions in the methane-ethane-propane-nitrogen-acetylene system on Titan, *Geochim. Cosmochim. Acta*, *115*, 217–240, doi:10.1016/j.gca.2013.03.030.

Graves, S. D. B., C. P. McKay, C. A. Griffith, F. Ferri, and M. Fulchignoni (2008), Rain and hail can reach the surface of Titan, *Planet. Space Sci.*, *56*, 346–357, doi:10.1016/j.pss.2007.11.001.

Hayes, A., et al. (2008), Hydrocarbon lakes on Titan: Distribution and interaction with a porous regolith, *Geophys. Res. Lett.*, *35*, L09204, doi:10.1029/2008GL033409.

Hayes, A., et al. (2010), Bathymetry and absorptivity of Titan's Ontario Lacus, *J. Geophys. Res.*, *115*, E09009, doi:10.1029/2009JE003557.

Hayes, A. G. (2016), The lakes and seas of Titan, *Annu. Rev. Earth Planet. Sci.*, *44*, doi:10.1146/annurev-earth-060115-012247.

Hayes, A. G., et al. (2011), Transient surface liquid in Titan's polar regions from Cassini, *Icarus*, *211*, 655–671.

Hofgartner, J., et al. (2014), The discovery of transient features in a Titan sea, *Nat. Geosci.*, *7*, 493–496.

Janssen, M. A., et al. (2009), Titan's surface at 2.2-cm wavelength imaged by the Cassini RADAR radiometer: Calibration and first results, *Icarus*, *200*, 222–239, doi:10.1016/j.icarus.2008.10.017.

Janssen, M. A., et al. (2016), Titan's surface at 2.18-cm wavelength imaged by the Cassini RADAR radiometer: Results and interpretations through the first ten years of observation, *Icarus*, doi:10.1016/jicarus.2015.09.027, in press.

Jennings, D. E., et al. (2016), Surface temperatures on Titan during northern winter and spring, *AstroPhys. J. Lett.*, *816*, L17.

Jiang, Y. Y., and P. Zhang (2011), Density determination of slush nitrogen by the improved capacitance-type densimeter, *Exp. Ther. Fluid Sci.*, *35*, 328–337.

Krasnopolsky, V. A. (2009), A photochemical model of Titan's atmosphere and ionosphere, *Icarus*, *201*, 226–256, doi:10.1016/j.icarus.2008.12.038.

Lamb, J., and A. Turney (1949), The dielectric properties of ice at 1.25 cm. wavelength, *Proc. Phys. Soc. Sect. B*, *62*(4), 272–273.

Lavvas, P. P., A. Coustenis, and I. M. Vardavas (2008), Coupling photochemistry with haze formation in Titan's atmosphere. Part II: Results and validation with Cassini/Huygens data, *Planet. Space Sci.*, *56*, 67–99, doi:10.1016/j.pss.2007.05.027.

Le Gall, A., et al. (2011), SAR, radiometry, scatterometry and altimetry observations of Titan's dune fields, *Icarus*, *213*, 608–624.

Le Gall, A., A. G. Hayes, R. Ewing, M. A. Janssen, J. Radebaugh, C. Savage, P. Encrenaz, and the Cassini Radar Team (2012), Latitudinal and altitudinal controls of Titan's dune field morphometry, *Icarus*, *217*, 231–242.

Leese, M. R., R. D. Lorenz, B. Hathi, and J. C. Zarnecki (2012), The Huygens surface science package (SSP): Flight performance review and lessons learned, *Planet. Space Sci.*, *70*(1), 28–45.

Levenberg, K. (1944), A method for the solution of certain problems in least-squares, *Q. Appl. Math.*, *2*, 164–168.

Lopes, R. M. C., et al. (2016), Nature, distribution, and origin of Titan's undifferentiated plains, *Icarus*, doi:10.1016/j.icarus.2015.11.034, in press.

Lorenz, R. D. (1998), Preliminary measurements of the cryogenic dielectric properties of water-ammonia ices: Application to radar observations of icy satellites, *Icarus*, *136*, 344–348.

Lorenz, R. D. (2014), The flushing of Ligeia: Composition variations across Titan's seas in a simple hydrological model, *Geophys. Res. Lett.*, *41*, 5764–5770, doi:10.1002/2014GL061133.

Lorenz, R. D. (2015a), Voyage across Ligeia Mare: Mechanics of sailing on the hydrocarbon seas of Saturn's moon, Titan, *Ocean Eng.*, *104*, 119–128.

Lorenz, R. D. (2015b), How I came to design extraterrestrial robot submarines. Part 2: Sailing Ligeia, diving Kraken, *SERVO*, *13*(6), 38–44.

Lorenz, R. D., and J. I. Lunine (1996), Erosion on Titan: Past and present, *Icarus*, *196*, 79–91.

Lorenz, R. D., and S. E. Shandera (2001), Physical properties of ammonia-rich ice: Application to Titan, *Geophys. Res. Lett.*, *28*, 215–218, doi:10.1029/2000GL012199.

Lorenz, R. D., G. Biolluz, P. Encrenaz, M. A. Janssen, R. D. West, and D. O. Muhleman (2003), Cassini RADAR: Prospects for Titan surface investigations using the microwave radiometer, *Planet. Space Sci.*, *51*(4–5), 353–354.

Lunine, J. I., D. J. Stevenson, and Y. L. Yung (1983), Ethane ocean on Titan, *Science*, *222*, 1229–1230.

Malaska, M. J., and R. Hodyss (2014), Dissolution of benzene, naphthalene, and biphenyl in a simulated Titan lake, *Icarus*, *242*, 74–81, doi:10.1016/j.icarus.2014.07.022.
Marquardt, D. (1963), An algorithm for least-squares estimation of nonlinear parameters, *SIAM J. Appl. Math.*, *11*, 431–444.
Mastrogiuseppe, M., et al. (2014), The bathymetry of a Titan sea, *Geophys. Res. Lett.*, *41*, 1432–1437, doi:10.1002/2013GL058618.
Mitchell, K. L., M. B. Barmatz, C. S. Jamieson, R. D. Lorenz, and J. I. Lunine (2015), Laboratory measurements of cryogenic liquid alkane microwave absorptivity and implications for the composition of Ligeia Mare, Titan, *Geophys. Res. Lett.*, *42*, 1340–1345, doi:10.1002/2014GL059475.
Mitri, G., et al. (2014), The exploration of Titan with an orbiter and a lake probe, *Planet. Space Sci.*, *104*, 78–92.
Mousis, O., J. I. Lunine, A. G. Hayes, and J. D. Hofgartner (2015), The fate of ethane in Titan's hydrocarbon lakes and seas, *Icarus*, doi: 10.1016/j.icarus.2015.06.024, in press.
Neish, C. D., Á. Somogyi, J. I. Lunine, and M. A. Smith (2009), Low temperature hydrolysis of laboratory tholins in ammonia-water solutions: Implications for prebiotic chemistry on Titan, *Icarus*, *201*, 412–421, doi:10.1016/j.icarus.2009.01.003.
Niemann, H. B., S. K. Atreya, J. E. Demick, D. Gautier, J. A. Haberman, D. N. Harpold, W. T. Kasprzak, J. I. Lunine, T.C. Owen, and F. Raulin (2010), Composition of Titan's lower atmosphere and simple gas volatiles as measured by the Cassini-Huygens probe gas chromatograph mass spectrometer experiment, *J. Geophys. Res.*, *115*, E12006, doi:10.1029/2010JE003659.
Paillou, P., K. Mitchell, S. Wall, G. Ruffie, C. Wood, R. Lorenz, E. Stofan, J. Lunine, R. Lopes, and P. Encrenaz (2008), Microwave dielectric constant of liquid hydrocarbons: Application to the depth estimation of Titan's lakes, *Geophys. Res. Lett.*, *35*, L05202, doi:10.1029/2007GL032515.
Press, W. H., et al. (1988), *Numerical Recipes in C: The Art of Scientific Computing*, Cambridge Univ. Press, New York.
Raulin, F. (1987), Organic chemistry in the oceans of Titan, *Adv. Space Res.*, *7*(5), 71–81.
Singh, S. P., and R. C. Miller (1978), Compressed-liquid dielectric constants and derived excess volumes for simple liquid mixtures: $N_2 + CH_4$ and $Ar + CH_4$, *J. Chem. Thermodyn.*, *10*, 747–763.
Sloan, E. D., and C. A. Koh (2008), *Clathrate Hydrates of Natural Gases*, 3rd ed., CRC Press, Taylor and Francis, Boca Raton, Fla.
Smith, P. A., L. E. Davis, T. W. Button, and N. McN Alford (1990), The dielectric loss tangent of liquid nitrogen, *Supercond. Sci. Technol.*, *4*, 128–129.
Stevenson, D. J., and B. E. Potter (1986), Titan's latitudinal temperature distribution and seasonal cycle, *Geophys. Res. Lett.*, *13*, 93–96, doi:10.1029/GL013i002p00093.
Stofan, E., R. Lorenz, J. Lunine, E. Bierhaus, B. Clark, P. Mahaffy and M. Ravine (2013), TiME—The Titan Mare Explorer, in *IEEE Aerospace Conference*, pp. 1–10, IEEE, Big Sky, Mont., doi:10.1109/AERO.2013.6497165
Stofan, E. R., et al. (2007), The lakes of Titan, *Nature*, *445*, 61–64, doi:10.1038/nature05438.
Tan, S. P., J. S. Kargel, and G. M. Marion (2013), Titan's atmosphere and surface liquid: New calculation using statistical associating fluid theory, *Icarus*, *222*, 53–72, doi:10.1016/j.icarus.2012.10.032.
Tan, S. P., J. S. Kargel, D. Jennings, M. Mastrogiuseppe, H. Adidharma, and G. M. Marion (2015), Titan's liquids: Exotic behavior and its implications on global fluid circulation, *Icarus*, *250*, 64–75.
Tobie, G., O. Grasset, J. I. Lunine, A. Mocquet, and C. Sotin (2005), Titan's internal structure inferred from a coupled thermal–orbital model, *Icarus*, *175*, 496–502, doi:10.1016/j.icarus.2004.12.007.
Tobie, G., J. I. Lunine, and C. Sotin (2006), Episodic outgassing as the origin of atmospheric methane on Titan, *Nature*, *440*, 61–64, doi:10.1038/nature04497.
Tokano, T. (2009), Limnological structure of Titan's hydrocarbon lakes and its astrobiological implication, *Astrobiology*, *9*, 147–164.
Tokano, T., and R. D. Lorenz (2015), Sun-stirred Kraken Mare: Circulation in Titan's seas induced by solar heating and methane precipitation, *Icarus*, doi:10.1016/j.icarus.2015.08.033, in press.
Turtle, E. P., J. E. Perry, A. S. McEwen, A. D. Del Genio, J. Barbara, R. A. West, D. D. Dawson, and C. C. Porco (2009), Cassini imaging of Titan's high-latitude lakes, clouds, and south-polar surface changes, *Geophys. Res. Lett.*, *36*, L02204, doi:10.1029/2008GL036186.
Turtle, E. P., et al. (2011), Shoreline retreat at Titan's Ontario Lacus and Arrakis Planitia from Cassini Imaging Science Subsystem observations, *Icarus*, *212*, 957–959.
Ulaby, F. T., R. K. Moore, and A. K. Fung (1982a), *Microwave Remote Sensing: Active and Passive*, *Microwave Remote Sens. Fundam. and Radiometry*, vol. I, Artech House, Norwood, Mass.
Ulaby, F. T., R. K. Moore, and A. K. Fung (1982b), *Microwave Remote Sensing: Active and Passive*, *Radar Remote Sens. and Surf. Scattering and Emiss. Theory*, vol. II, 830 pp., Artech House, Norwood, Mass.
Wye, L., H. Zebker, and R. Lorenz (2009), Smoothness of Titan's Ontario Lacus: Constraints from Cassini RADAR specular reflection data, *Geophys. Res. Lett.*, *36*, L16201, doi:10.1029/2009GL039588.
Zebker, H., A. G. Hayes, M. Janssen, A. Le Gall, R. Lorenz, and L. Wye (2014), Surface of Ligeia Mare, Titan, from Cassini altimeter and radiometer analysis, *Geophys. Res. Lett.*, *41*, 308–313, doi:10.1002/2013GL058877.